

Effects of Dimples on Aerodynamic Performance of Horizontal Axis Wind Turbine Blades

Gedyon Fikade^a, Addisu Bekele^{b,*}, Chandrababu Venkatachalam^b and Mohanram Parthiban^c

^aM.Sc. Mechanical Engineering Department, Adama Science and Technology University, Adama, Ethiopia

^bAssistant Professor, Mechanical Engineering Department, Adama Science and Technology University, Adama, Ethiopia

^cLecturer, Mechanical Engineering Department, Adama Science and Technology University, Adama, Ethiopia

Abstract - Wind energy is one of the fast growing power industry and promising renewable energy source in the world. Wind turbine technology is a system that converts kinetic energy of the wind into electrical energy. The main purpose of this study is to investigate the aerodynamic effect of dimples over the surface of a horizontal axis wind turbine (HAWT) blades.

The National Renewable Energy Laboratory's (NREL) S830 model wind turbine blade is selected for this study. Among the different methods of blade design, Blade Element Momentum (BEM) theory is used to optimize the chord and twist distributions of the blades. The aerodynamic performance of the designed blade is examined using commercially available Computational Fluid Dynamic (CFD) software known as ANSYS FLUENT. Due to its ability to capture flow separation and accuracy, Large Eddy Simulation (LES) transient turbulence model is selected and used to simulate the computational model. A number of dimple with different configurations are added on pressure and suction side of the blade surface and their corresponding effects on the aerodynamic performance of the turbine are studied.

Validation of the computational result is done by using an experimental test of scaled down S830 model under sub-sonic wind tunnel. Both numerical and experimental results show that aerodynamic performance of dimpled wind turbines are enhanced by delaying the flow separation.

Based up on the cetin correlation the power extraction coefficient of designed base model blade is found to be 0.41 whereas that of dimples blade with Config#2 is obtained to be 0.4415.

Key Words: Wind Turbine Blade, Surface Dimple, S830 Airfoil, Aerodynamic Performance, CFD.

1. INTRODUCTION

The world demand for renewable energy is growing fast because of the rapid climate change and limited amount of fossil fuels. Wind turbine is one of the fastest growing technologies globally at an average annual growth rate of more than 26% since 1990. (Usha and Kishore, 2009).

Two major types of wind turbines exist based on their blade configuration and operation. The first kind is the horizontal axis wind turbine (HAWT). This kind of wind turbine is the most common and can often be seen scattered across the landscape in areas of relatively level terrain with predictable year round wind conditions. These wind turbines have been the main subject of wind turbine research for decades, mainly because they share common operation and dynamics with rotary aircraft. A combination of the lift and drag causes the rotor to spin. This turns the generator and produce electricity.

The second major type of wind turbine is the vertical axis wind turbine (VAWT). This kind of wind turbine turns around an axis that is perpendicular to the upcoming stream; hence, it can take wind from any direction.

According to the analysis of Lanchester and Betz the maximum possible amount of energy extraction from a wind by wind turbine is 59.3% of the incoming kinetic energy (Betz, 1930). Nevertheless, most wind turbines can't achieve this efficiency. The common challenge for the wind turbine designer is to maximize the energy capture within the given restrictions (White, 2009). The main incentive of blade rotation is the lift force created by pressure difference in the flow over of airfoils. Contemporary research findings reveal that dimples on the surface of aircraft's airfoils enhance the aerodynamic efficiency and maneuverability of the aircraft by mitigating stall. (Srivastav, 2012 and Livya et al., 2015). This study numerically investigates the configurations of suitable dimples for HAWT blades, examine the aerodynamic characteristics of the designed

* Corresponding Author

Email: addisu2009@gmail.com

blade without dimples, aerodynamic effect of dimples on surface of wind turbine blade and compare the power extraction coefficient of the baseline turbines with the dimpled one. Also experimental validation of the numerical result has been done.

2. LITERATURE REVIEW

2.1 Wind Turbine Blade Design

Mulugeta (2009) studied computer-aided aerodynamic and structural design of horizontal axis wind turbine blades. In his paper detailed review of the designing horizontal-axis wind turbine (HAWT) blades to achieve satisfactory levels of performance is given. HAWT blade design was studied from the aspect of aerodynamic view. BEM method is selected for the blade design. Additionally the basic principles of the aerodynamic behaviors of HAWTs was investigated.

Haseeb et al. (2014) studied on Low Reynolds Number Airfoil for Small Horizontal Axis Wind Turbine Blades. In this study a direct design method is employed for small horizontal axis wind turbines operating at low wind speeds and consequently at lower Reynolds numbers (Re). Post-design viscous study tool 'Xfoil' is used for optimization of the airfoil. The aim is to attain higher values of lift-to-drag ratio (L/D ratio) for the tip of the blades. The new airfoil, named 'UBD-5494', was tested in 'Xfoil' with Re in the range of 30 000, 55 000, 70 000, and 100000. Each of these situations are analyzed at various angles of attack, ranging from 0 to 20 degrees at one degree increments. Performances of other existing airfoil options are also compared with 'UBD-5494'. The new airfoil shows distinctively higher efficiency in comparison to other existing airfoils at low Re in terms of Lift-to-drag ratio at its design lift coefficient and is therefore recommended for tip of small horizontal axis wind turbine blades

Peter and Richard (2012) presented the detailed review of the current state-of art for wind turbine blade design, including theoretical maximum efficiency, propulsion, practical efficiency, HAWT blade design, and blade loads. The review was provided a complete picture of wind turbine blade design and shows the dominance of modern turbines almost exclusive use of horizontal axis rotors. The aerodynamic design principles for a modern wind turbine blade are detailed including the blade plan shape/quantity, airfoil selection and optimal attack angles, described aerodynamic, gravitational, centrifugal, gyroscopic and operational conditions

Serhat, (2005) studied computer- aided design of horizontal- axis wind turbine blades. In this paper, HAWT blade design was studied from the aspect of aerodynamic view and the basic principles of the aerodynamic behaviors of HAWTs are investigated. Blade-element momentum theory (BEM) known as also strip theory, that is the current mainstay of aerodynamic design and analysis of HAWT blades, is used for HAWT blade design in this paper. Firstly, blade design procedure for an optimum rotor according to BEM theory is performed. Then designed blade shape was modified such that modified blade will be lightly loaded regarding the highly loaded of the designed blade and power prediction of modified blade was analyzed. When the designed blade shape was modified, it has seen that the power extracted from the wind was reduced about 10% and the length of modified blade was increased about 5% for the same necessitated power.

Port-Agel, et al., (2011): Even if RANS simulations can achieve accurate and meaningful outcomes they only calculate the mean flow and parameterize the scales of turbulence for more accurate and descriptive results LES simulations are necessitated. LES models employ a filter based on grid size so that where the mesh is fine enough the stream is resolved, similar to direct numerical simulation (DNS), and where the mesh size is too coarse, a SGS turbulence closure scheme is employed to model the flow. Following this performed a LES study using a tuning-free Lagrangian dynamic. SGS model recently developed for wind energy applications to model both single turbine wakes and wake interactions in an operating wind farm

As these literature reviews illustrate, there are many different numerical solutions to the Navier-Stokes equations that have been implemented successfully for HAWT. Of the RANS closure models, the $k-\omega$ SST model was seen to have the most success. With respect to LES, the tuning-free SGS models were the most widely employed. Conversely, LES necessitates a very fine grid resolution to not over burden the SGS model. A method to mitigate large mesh sizes is the widely employed actuator disk model (ADM). A variety of ADMs exist, but the best results were found among those formulated using the BEM method over a disk or actuator lines.

2.2 Concept of Dimple

The Concept of dimples arrive from golf balls. Golf balls have inner dent in form of dimples on their outer surfaces. These dimples aid golf balls to lower drag. A liquid streaming over a protest tends to drag the question along its stream bearing. A question going through a liquid that is stationary there is a tendency to back the protest off. For a stationary question in a liquid that is streaming there is an inclination to move the protest in the liquid streaming heading. This tendency of streaming liquid is known as drag. As dimples reduce drag of golf ball they can be useful on reducing wings drag. That grows the attention of several researchers about dimple. There were a lot of experiments and numerical investigations have been conducted by several researchers around the world on dimpled effect on airplane wings, golf ball and as a way to enhance heat transfer.

Arun, *et al.* (2018) on their work proved this “The predominant factors influencing the efficiency of the wind turbines are lift and drag that are to be maximized and minimized respectively. Surface of turbine blades are included with dimples of various sizes and arrangements and are analyzed using CFD to obtain an optimum combination, through that efficiency of wind turbines can be maximized”. According to their work Nearly 1.36 MW power was found to be generated and with high levels of accuracy on comparison with actual values, preceded towards the inclusion of dimples; Based on the pressure contour obtained. Dimples are included on the high pressure (bottom side) of the turbine. Further analysis with dimples have increased the performance to a greater extent, about 1.56 MW power was found to be generated, a 14.5% increase in performance, to be precise. Thus, inclusion of dimples on the surface of wind turbine blades will increase performance levels.

3. BLADE DESIGN ANALYSIS

The aerodynamic design of a wind turbine rotor includes the choice of the number of blades, determination of blade length, type of airfoil section, blade chord and twist distributions and the design tip-speed ratio (*TSR*). A rotor with one blade can be cheaper and easier to erect but it is not popular and too noisy. The two-bladed rotor is also simpler to assemble and erect but produces less power than that developed by the three-bladed one. The latter produces smoother power output with balanced gyroscopic loads, and is more aesthetic.

The determination of the blade length (or rotor size) depends mainly on the needed energy for certain application and average wind speed of a specific site. The choice of the kind of airfoil section may be regarded as a key point in designing an efficient wind rotor (Burger and Hartfield, 2006).

In this paper, Blade momentum theory (BEM) is used to design a HAWT blade based up on the wind data analysis of a specific location (9.222° latitude, 41.790° longitude), the energy density of the site is found to be 610 w/m². BEM is employed for obtaining maximum lift to drag ratio for each elemental constitution of the blade. Obtaining chord and twist distribution at selected tip speed ratio of the blade, the aerodynamic shape of the blade in every part is specified with correspond to maximum accessible power coefficient. The design parameters are power coefficient, angle of attack, drag and lift coefficients.

For wind turbine blade design and analysis, it is essential to have the aerodynamic data of the selected airfoil at the corresponding flow conditions.

Reynolds Number (Re): The Reynolds number is defined as:

$$R_e = \frac{U_{rel} C}{\nu} \quad (2)$$

Where: U_{rel} is the relative wind speed (m/s).

C is chord length (m).

ν is kinematic viscosity of air ($\nu = 14 \times 10^{-6} \text{ m}^2/\text{s}$)

Tip Speed Ratio: - The tip speed ratio is defined as the relationship between rotor blade velocity and relative wind velocity. It is the foremost design parameter around which all other optimum rotor dimensions are calculated: (Hansen and Butterfield, 1993)

$$\lambda = \frac{\Omega r}{V_w} \quad (3)$$

Where: λ = Tip speed ratio Ω_r = Rotational velocity (rad/s), r = radius, V_w = Wind speed.

Features such as efficiency, torque, mechanical stress, aerodynamics and noise should be considered in selecting the appropriate tip speed.

A higher tip speed demands lessen chord widths leading to narrow blade profiles. This can steer to reduce material usage and lower production costs. Even if an increase in centrifugal and aerodynamic forces is linked with higher tip speeds. The increased forces imply that difficulties exist with maintaining structural integrity and avoid blade failure. As the tip speed increases the aerodynamics of the blade design become increasingly critical. A blade which is designed for great relative wind speeds develops minimal torque at lower speeds. This results in a higher cut in speed and difficulty self-starting. A noise increase is also associated with increasing tip speeds as noise increases approximately proportionately to the sixth power. Modern HAWT generally utilize a tip speed ratio of 9 - 10 for two bladed rotors and 6 - 9 for three blades. This has been found to produce efficient conversion of the winds kinetic energy into electrical power (Peter, et al. 2012).

The Betz method gives the basic shape of the modern wind turbine blade (Figure 1). (Hansen and Butterfield, 1993)

$$C_{opt} = \frac{2\pi r}{n} \frac{8 U_{wd}}{9 C_L \lambda V_r} \tag{4}$$

Where, $V_r = \sqrt{V_w^2 + U^2}$

r = radius (m),

n = Blade quantity,

C_L = Lift coefficient, λ = Local tip speed ratio,

V_r = Local resultant air velocity (m/s),

U = Wind speed (m/s)

U_{wd} = Design wind speed (m/s),

C_{opt} = Optimum Chord length

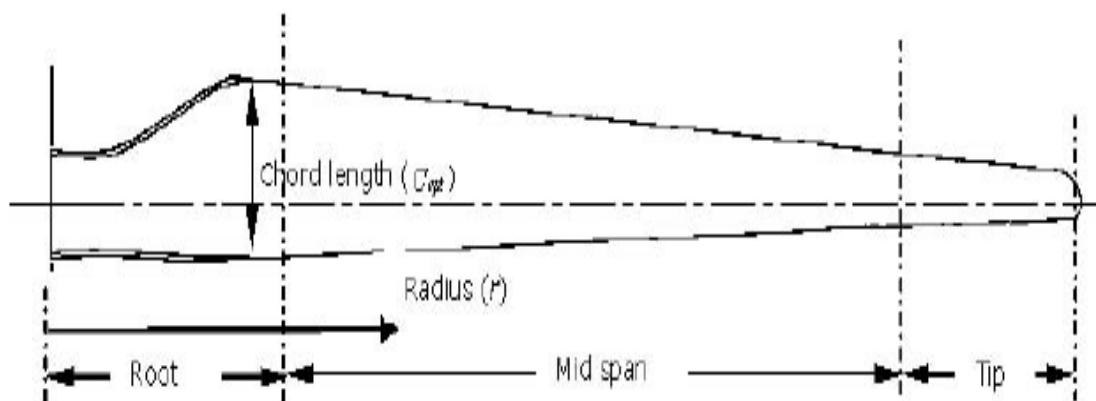


Figure 1: Nomenclature of wind turbine blade

Assuming that a reasonable lift coefficient is maintained, utilizing a blade optimization method produces blade plans principally dependent on design tip speed ratio and number of blade. For this work based up on the wind potential it's feasible to employ 25 m span blade and TSR value of 6.75.

Turbines are designed to operate within a specific range of wind speeds. Based on the selected site cut in wind speed 3 m/s, cut off wind speed 22 m/s and rated wind speed 10m/s are selected. Tangential speed of blade vary across the span of blade amount lift vary across the blade span. In order to have a uniform lift coefficient the chord distribution of the blade vary from the root to tip. By using BEM method the chord distribution result along the span is plotted on **Figure 2**.

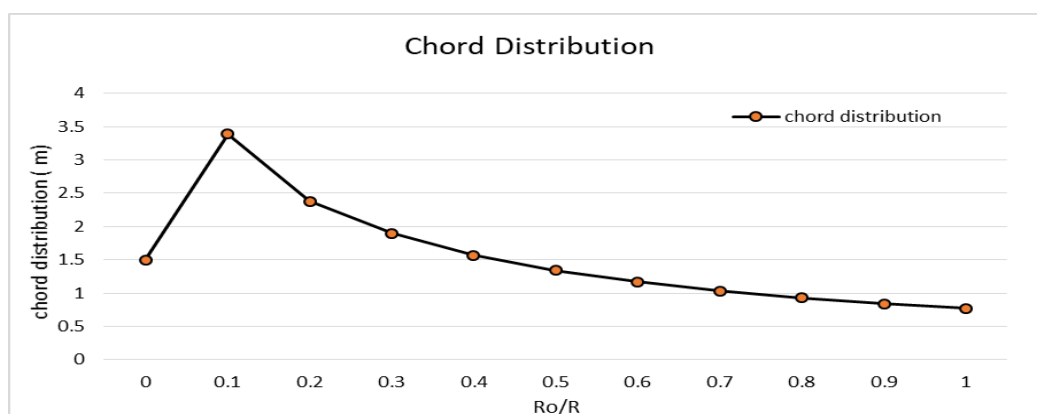


Figure 2: Chord Distribution versus Span Length Ratio

BEM method employs blade twist angle is calculated from; (Hansen and Butterfield, 1993)

$$\varphi = \left(\frac{2}{3}\right) \tan^{-1} \left(\frac{1}{\lambda_r}\right) \tag{5}$$

Where: λ_r is the local speed ratio, φ is the blade twist angle.

The justification for the twist is to produce uniform lift from the hub to the tip. As the blade rotates, there is a difference in the actual speed of the various portions of the blade. The tip of the blade travels faster than the part near the hub, because the tip travels a greater distance than the hub in similar length of time. **Figure 3** depict end result of the angle of twist based on the above mathematical correlation employed.

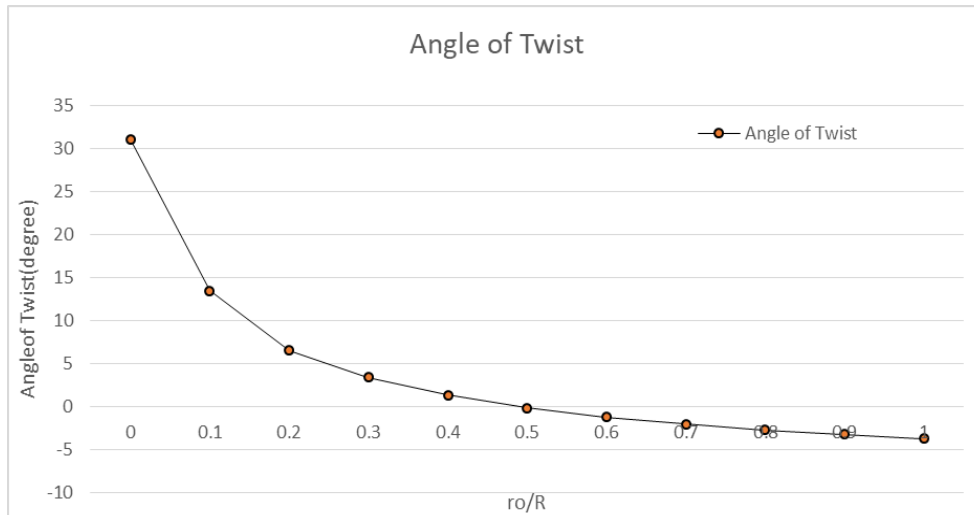


Figure 3: Angle of Twist versus Span Ratio

The **Figure 4** shows schematic and surface drawing of the chord distribution and angle of Twist of the designed blade using S830 airfoil.

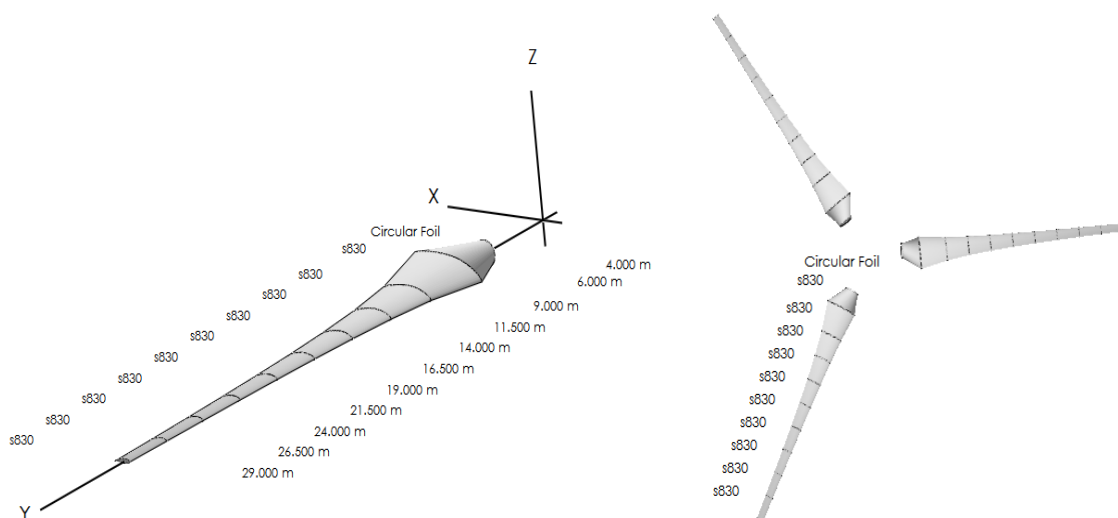


Figure 4: Schematic Drawing of Designed wind Turbine Blade

Aerodynamic lift is the force reliable for the power yield generated by the turbine and it is therefore essential to capitalize this force using appropriate design. A resistant drag force that counter the motion of the blade is also generated by friction which

must be lessen. It is then vivid that an airfoil section with a high lift to drag ratio, typically greater than 3, be chosen for rotor blade design (Hansen and Butterfield, 1993):

$$\text{Lift to Drag Ratio} = \frac{\text{Coefficient of lift}}{\text{Coefficient of drag}} = \frac{C_L}{C_D} \tag{6}$$

According to Betin, the power coefficient is a function of TSR, blade number and maximum lift/drag ratio (Peter and Richard, 2012)

$$C_p = \left(1 - \frac{\lambda}{c_l/c_d}\right) \times \left(1 - \frac{1.84}{z \cdot \lambda}\right) \tag{7}$$

Where: Z is the blade number, which is 3,

$\frac{C_L}{C_D}$ is the maximum lift to drag ratio

C_p is the Schmitz power coefficient, which is 0.5926.

4. COMPUTATIONAL MODEL

The geometry of the designed reference turbine was created in SolidWorks and exported into ANSYS DesignModeler, where the domain geometry is created. The domain was sized 15 m upstream of the turbine, 27m downstream of the first turbine, and 15m span wise on either side of the turbines. The total height of the domain was set to 30m as shown in the **Figure 5**. Eventually the whole model and flow tunnel was scaled down to a ratio of one to hundred.

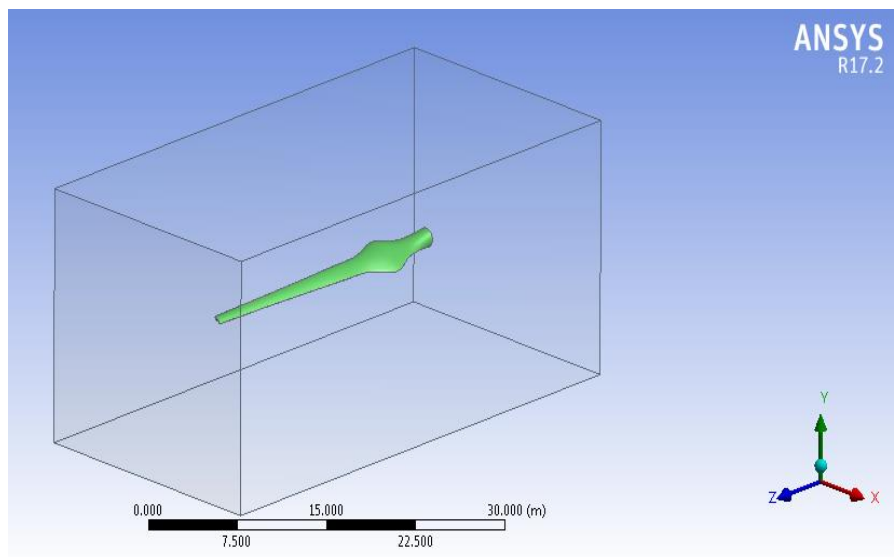


Figure 5: Baseline model in Virtual flow tunnel

For this study the reference baseline blade model and six different dimple orientation imparted on the baseline model are used.

The detail specification of each configuration is given in the Table 1 below.

Table 1: Specification of different configuration Models

Model Name	Span length	Airfoil type	Dimple specification	Location
Baseline	25m	S830	-	-
Config. One	25m	S830	10cm, outward	0.5 of chord length on the suction surface
Config. Two	25m	S830	10cm,inward	0.5 of chord length on the suction surface
Config. Three	25m	S830	5cm,outward	0.4 of chord length on the suction surface
Config. Four	25m	S830	5cm,inward	0.4 of chord length on the suction surface
Config. Five	25m	S830	10cm,outward	0.5 of chord length both on the suction and pressure surface
Config. Six	25m	S830	10cm,inward on pressure side and 0.5 inward at suction surface	0.5 of chord length on suction side & 0.8 of chord length on pressure side

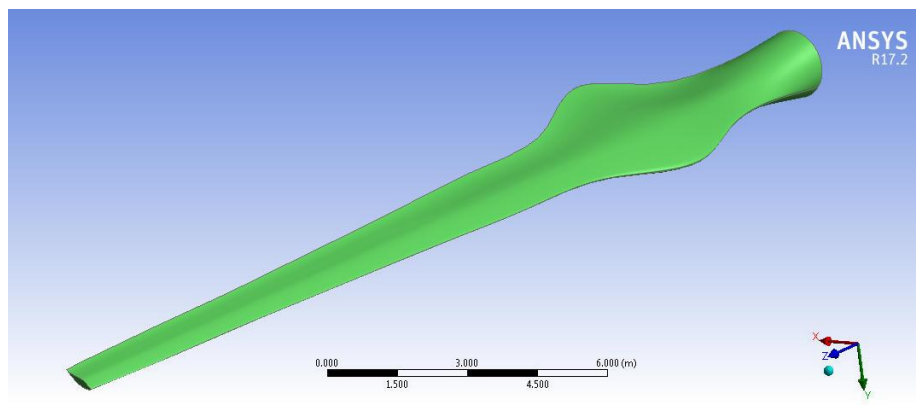


Figure 6: Baseline Model

Configuration number one, three and five (suction side) (Figure: 7, 9, and 12 resp.) include an outward dimple with a distinct diameter while, for configuration number two, four, five (pressure side) and six both side (Figure: 8, 10, 11, 13 and 14 resp.) inward dimples are imparted and the corresponding aerodynamic consequence is examined.

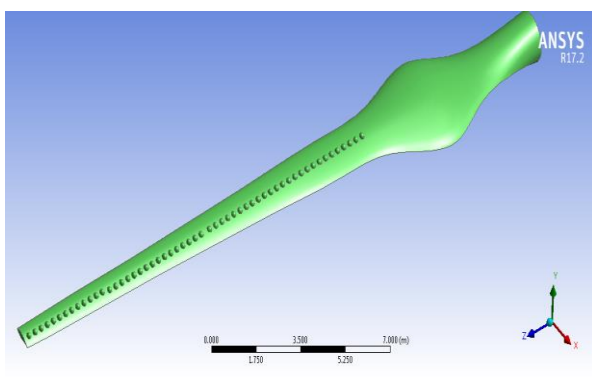


Figure 7: Blade with Dimple Orientation One.

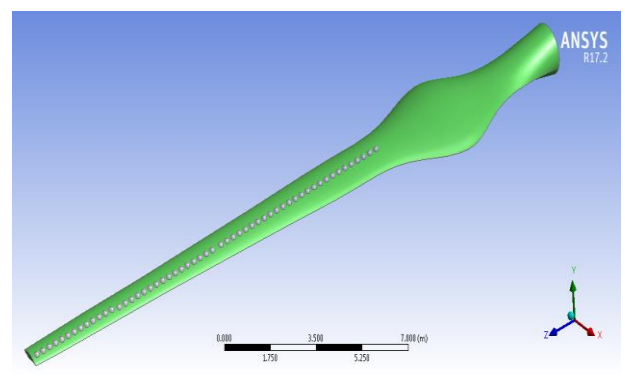


Figure 8: Blade with Dimple Orientation Two

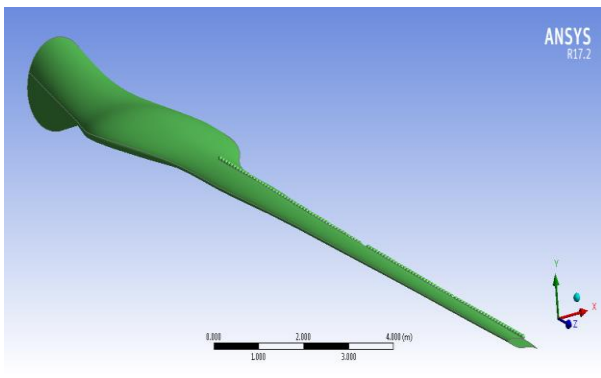


Figure 9: Blade with Dimple Orientation Three.

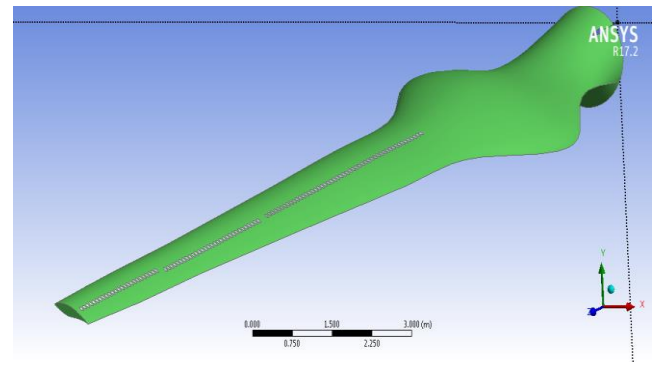


Figure 10: Blade with Dimple Orientation Four.

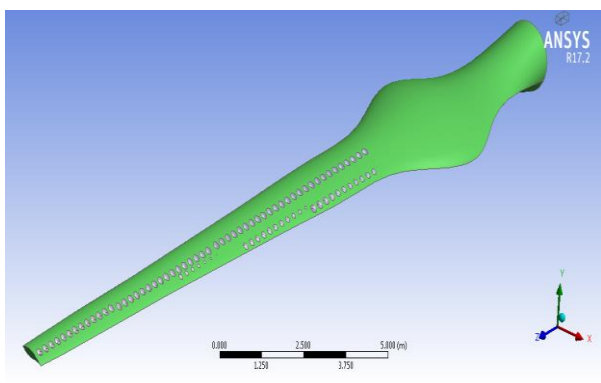


Figure 11: Blade with Dimple orientation Five (pressure side).

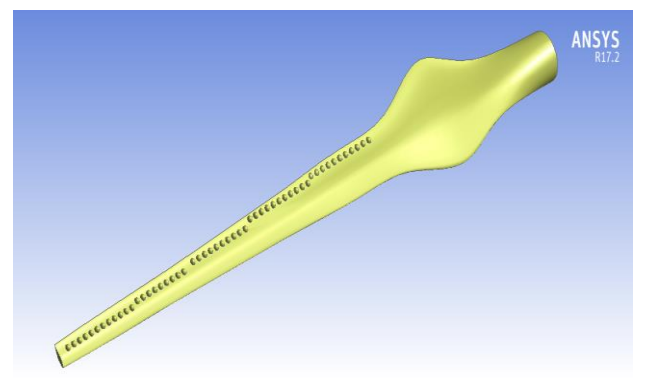


Figure 12: Blade with Dimple orientation Six suction face.

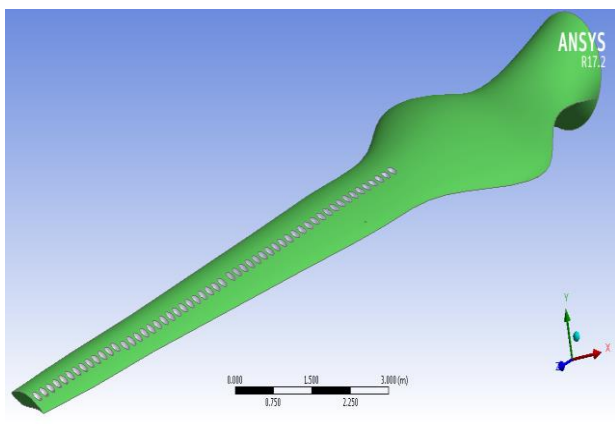


Figure 13: Blade with Dimple Orientation Six on pressure side.

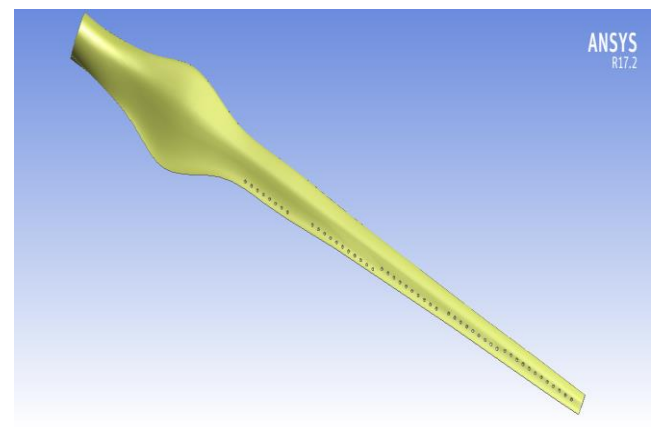


Figure 14: Blade with Dimple Orientation Six on Suction Side

5. MESHING THE MODEL

Meshing is performed using an unstructured tetrahedral mesh. After grid independency test is carried out the cell sizes were set to one millimeter on the blade faces, 0.5 millimeter on the blade tips. Cells were kept to a maximum size of 1 mill-meters in the horizontal directions and vertical direction. Inflation layers were implemented on all solid surfaces with a maximum growth rate of 1.2. The meshes of all variations of the stationary reference turbine contained approximately two million cells.

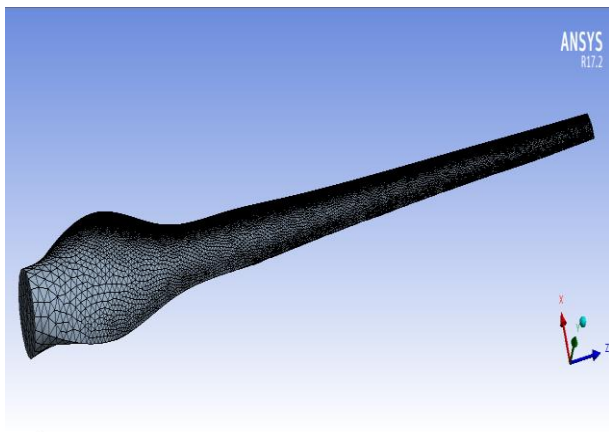


Figure 15: Mesh view on 3D Blade Surface.

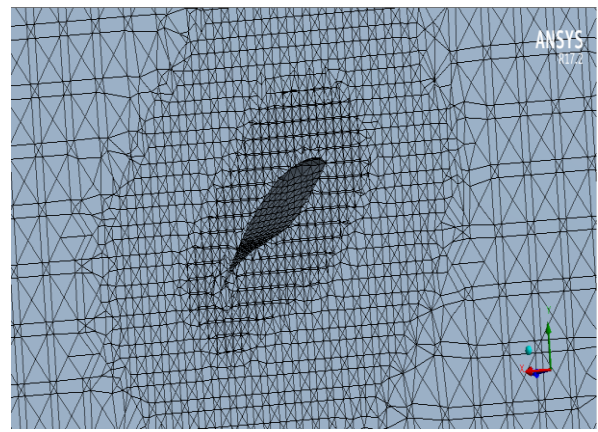


Figure 16: Zoom out view of a mesh near blade section which is refined mesh region on virtual flow tunnel

6. RESULTS AND DISCUSSIONS

6.1 Aerodynamic Characteristics of Baseline Blade

Aerodynamic characteristics of blade is essential to predict the extraction efficiency and flow phenomena. In this section the aerodynamic performance of the baseline (designed) blade is analyzed at a Reynolds number of 1.32×10^6 using LES turbulent model; Hence LES has superb potential to analyze and capture flow separation.

6.2.1 Pressure contour and velocity streamline

Wind turbine blade experience different flow phenomena with respect to distinct flow conditions. Angle of attack and velocity are primary factor which influence aerodynamic forces and the flow behavior. In this work the designed blade flow phenomena is examined by varying the angle of attack from -10° to 25° at a constant Reynolds number. The following plots shows pressure contour and velocity streamline along the designed blade; at various selected angle of attack.

As its shown in Figure 17 at verylow angle of attack (-5°) flow separation exist at pressure side of the blade, hence the blade will have a low lift to drag ratio. The lift and Drag coefficient are -0.09 and 0.26 respectively which is minor.

In the Figures 18 and 19 the fluid streamlines at an angle of attack of 5° and 10° are presented. As it's shown the fluid element reaching the leading edge reaches also the trailing edge hence there is no flow separation. As a consequence of that, the amount of lift force on the blade becomes high and Drag force is minimized. At $\alpha = 10^\circ$ ratio of the lift force to the drag force is 9.76 which is very good for wind turbine blades.

In the Figures 20, 21 and 22 the flow phenomena at an angle of attack of $\alpha=15^\circ$, $\alpha=20^\circ$ and $\alpha=25^\circ$ is presented. The figures vividly shows the fluid element reaching the leading age will not reach at the trailing age; in situations of lower α values the fluid element adhere to the surface starting from the leading edge to trailing edge. As the angle of attack of the blade is enhanced there is tendency of stall occurrence. For the baseline blade stall starts at an angle of attack of 15° around the tip section latter on if the angle of attack is further increased the stall will propagate throughout the blade and Eventually, no lift force will be generated.

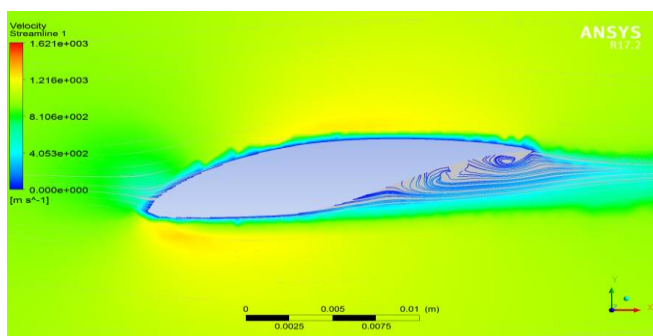


Figure 17: Velocity Streamline At $\alpha = -5^\circ$

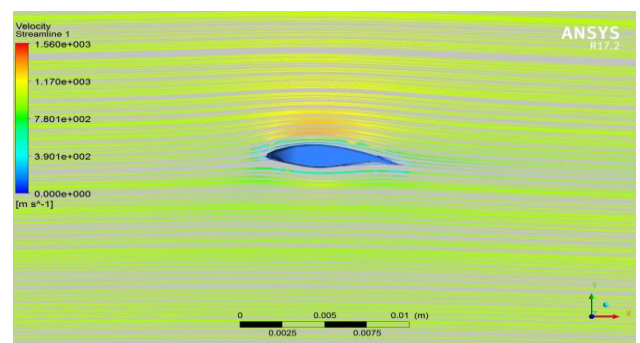


Figure 18: Velocity Streamline At $\alpha = 5^\circ$

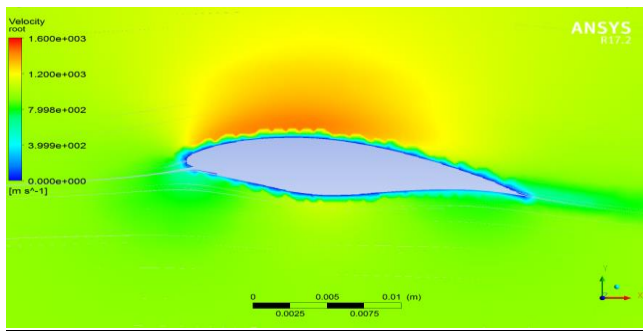


Figure 19: Velocity Streamline at $\alpha = 10^\circ$

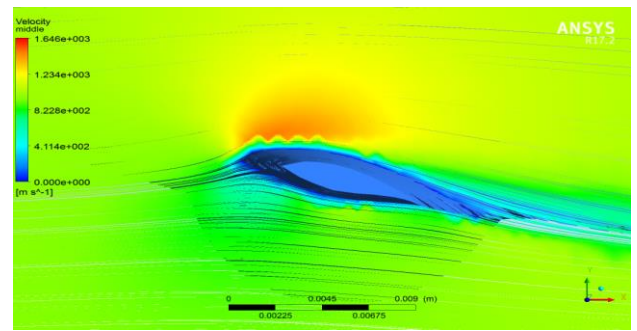


Figure 20: Attached Flow at Mid-Section at $\alpha = 15^\circ$

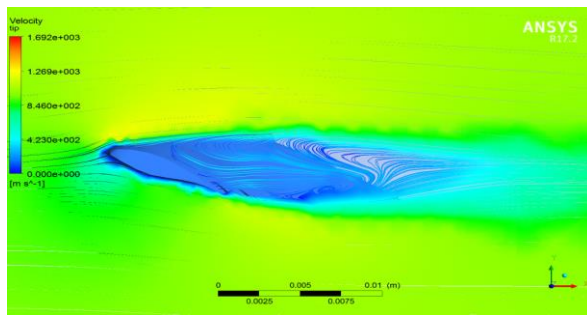


Figure 21: Velocity Streamline At Mid-Section $\alpha = 20^\circ$

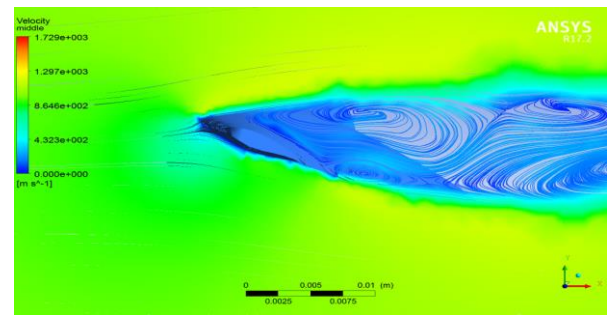


Figure 22: Velocity Streamline At Mid-Section $\alpha = 25^\circ$

Figure 23 and 24 Shows the pressure contour on the pressure side of the low angle of attack (-5°) and the high angle of attack ($\alpha = 25^\circ$) respectively.



Figure 23: Pressure Side Pressure Contour at $\alpha = -5^\circ$

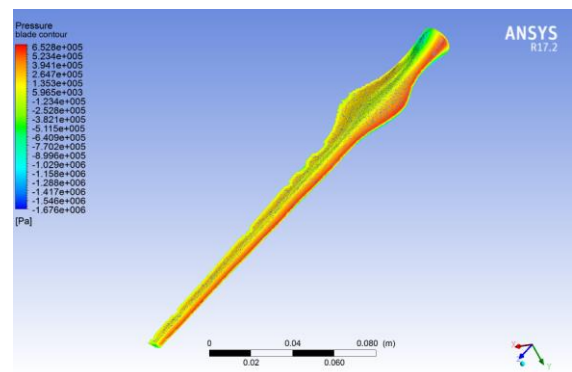


Figure 24: Pressure-Side Pressure Contour at $\alpha = 25^\circ$

Aerodynamic performance of wind turbine, vehicle, aircraft, or any other device or components is examined by calculating the ratio of lift force to drag force. The lift coefficient and drag coefficient of the designed blade at a different angle of attack is calculated using CFD results and presented hereunder. Figures 25 and 26 represent the lift coefficient; drag coefficient and aerodynamic performance of the baseline blade.

As illustrated in the above section flow separation on the designed wind turbine blade starts from an angle of attack of 15° . Figures 25 and 26 also demonstrate the decrement of lift force and aerodynamic performance after angle of attack of 15° due to stalling effect. Hence the designed wind turbine should operate at an angle of attack range of 3° to 12° .

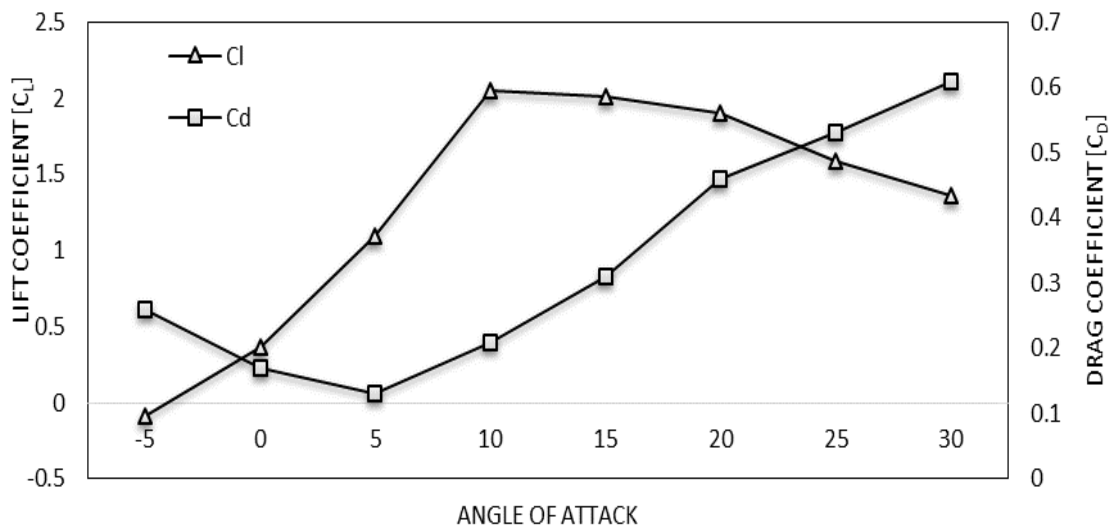


Figure 25: Lift and Drag Coefficient versus Angle of Attack

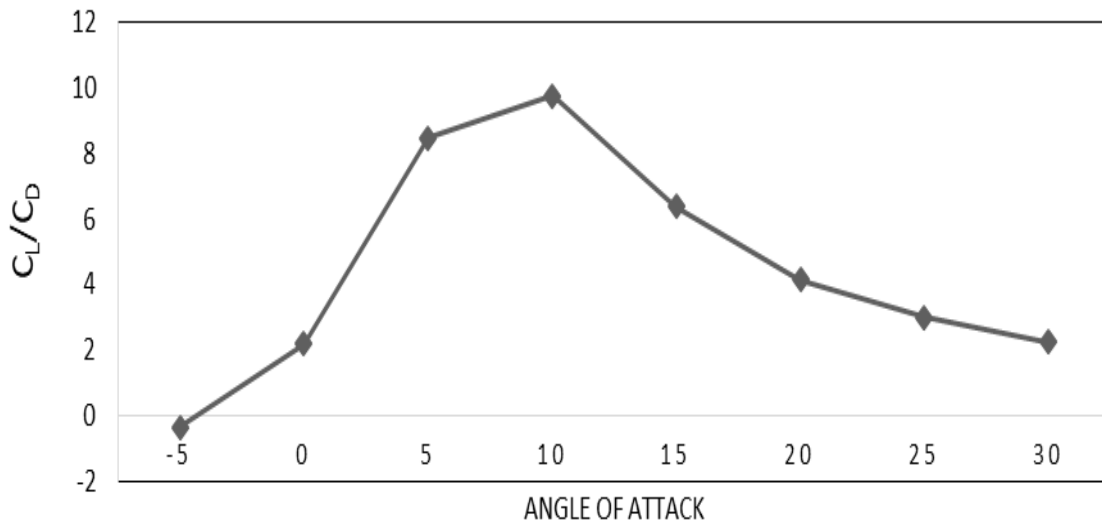


Figure 26: Aerodynamic Performance Versus Angle of Attack

6.2 Aerodynamic Characteristics of Blade with Dimples

In section 6.2 the aerodynamic characteristics of the designed blade were presented and the corresponding results shows that stall had mitigate the aerodynamic performance after an angle of attack of 15°. In this portion the evaluation result of different dimple configuration for delaying flow separation is presented.

Six different dimple configurations were studied after a preliminary parametric study on dimple. Both inward and outward dimples were studied.

In the first model (Figure 27) fifty five outward dimples with a diameter of 10 cm at a chord length ratio of 0.5 were imparted. The result explicate clearly that outward dimple will not delay flow separation rather they will induce additional drag force on the blade.

The second dimple orientation (Figure 28) consists of fifty eight inward dimples at half of the chord. The dimples were created with a diameter of 20 cm. The study results shows that this orientation have a very good result with respect to delaying flow separation. Consequently these dimple arrangements create a higher lift force than the baseline. The velocity streamline at an angle of attack of 17° is presented. The figure vividly illustrate dimples configuration number two had created an attached flow on the flow field.

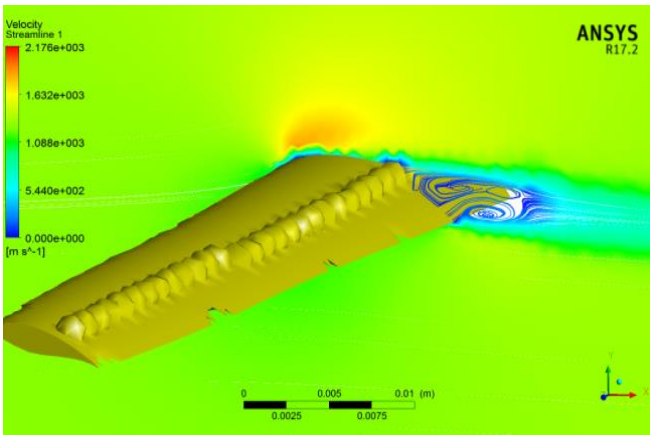


Figure 27: Separated Flow At $\alpha=15^\circ$ for Config. #1

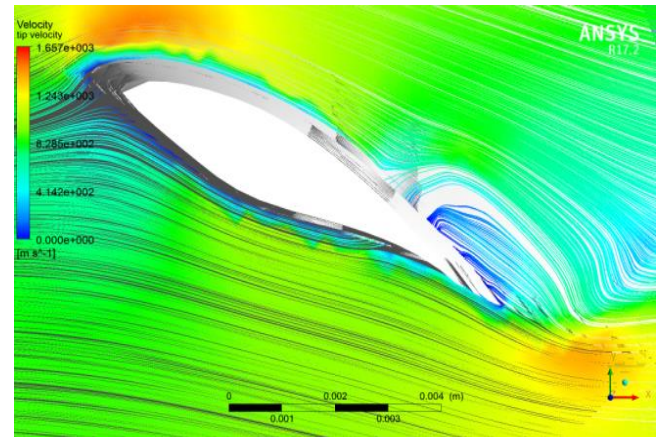


Figure 28: Config. #2 Velocity Streamline At $\alpha=17^\circ$

The third and fourth configuration models have 5cm outward and 5 cm inward dimples respectively. The location of the dimple for both situations is at 0.4 of the chord length. The study on these dimple arrangement shows that both dimple orientation have enhanced the lift force with a small value, while Dimple orientation number five and six have a different aspect than the previous four situations. CONFIG#5 and CONFIG#6 have surface dimples on both the suction surface and pressure surface; the previous four studies were on dimples at the suction side (low pressure surface) of the blade.

The aerodynamic performance of the fifth and sixth dimple arrangement shows that configuration six (Figure 29) possess good quality with regard to delaying flow separation while the fifth arrangement increase both the amount of drag and lift force.

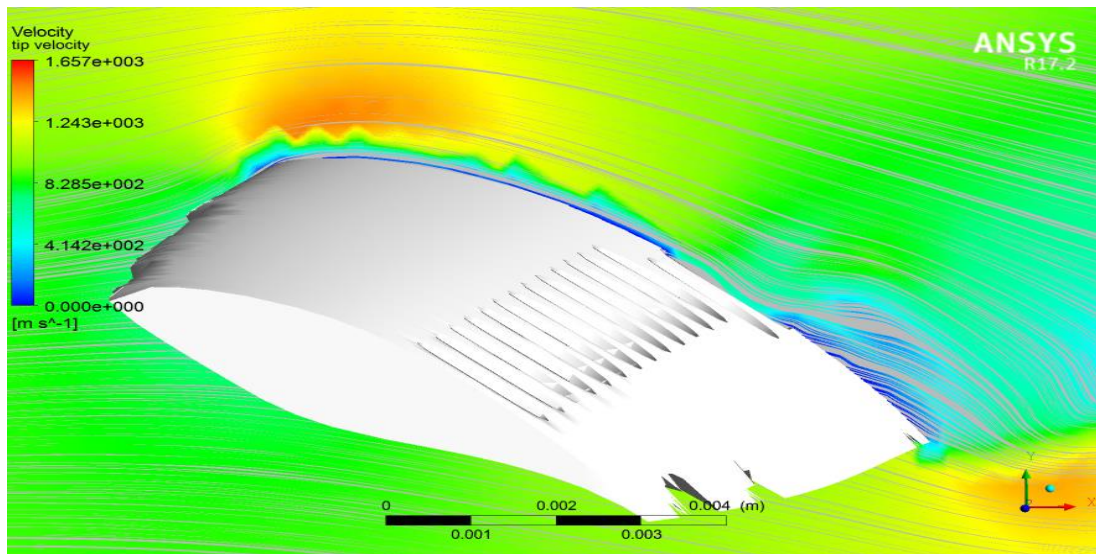


Figure 29: Config#6 Velocity Streamline at $\alpha=20$

Among these six different configuration of dimples; blade configuration number two and six showed a better result with regard to delaying flow separation.

The amount of lift force is directly related with the flow separation or attachment. Comparison of lift coefficient of wind turbine blade base model with the six distinct dimple arrangements is plotted in the Figure 30.

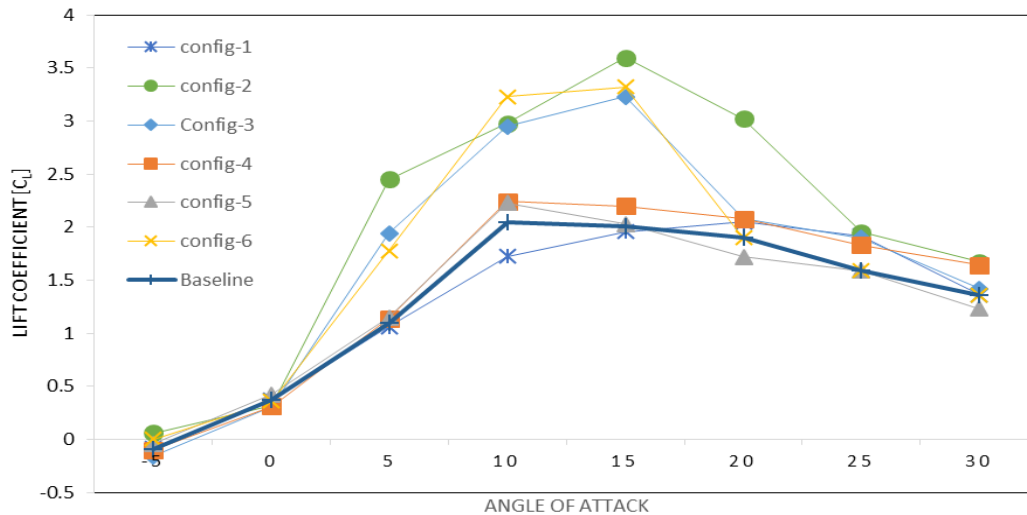


Figure 30: Comparison of Lift Coefficient of Baseline and Various Dimple Configurations

6.3 Performance Improvement on the Wind Turbine

Wind turbines' extraction efficiency is largely dependent up on the aerodynamic performance of the blade. In the previous sections the aerodynamic performance of the baseline blade and blade with different dimple configuration is presented. These results show that some dimple arrangement enhance the aerodynamic performance of a blade. In this section the effect of aerodynamic performance on the aggregate efficiency of wind turbine blade is analyzed and discussed.

Aerodynamic performance is the ratio of lift force to drag force. The aerodynamic performance of the baseline and blade with dimple is analyzed and the result shown in the Figure 31.

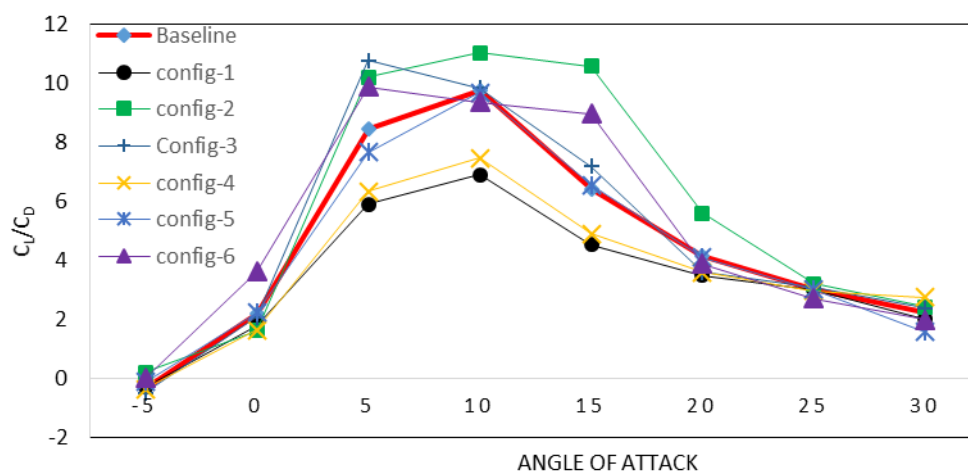


Figure 31: Aerodynamic Performance of Baseline and models with Various Dimple Arrangement

The power extraction coefficients of baseline and CONFIG#2 blades are analyzed by selecting number of blade as three. Using certain correlation the amount of power extraction coefficient (C_p) for designed base model blade becomes 0.4181 and for wind turbine with CONFIG#2 blade model the C_p value becomes 0.4467. Thus, CONFIG-2 wind turbine is preferred among the six different dimple configuration studied because of its higher aerodynamic performance.

6.4 Validation of the CFD result with Experimental one

CFD simulations are a very promising method for predicting the aerodynamic behavior of wind turbines in an inexpensive and accurate way. One of the major drawbacks of this method is the lack of validated models. For this study experimental result of small scaled S830 airfoil (Figure 32 & 33) is used for validating the computational work. Figure 34 shows experiematal and CFD result of S830 airfoil at a Reynold number of 114,234. The results show that the variation of lift coefficient among the CFD analysis and expermental evaluation ranges between 7 up to 12%. Therefore, it is possible conclude that the CFD results are within acceptable accuracy.

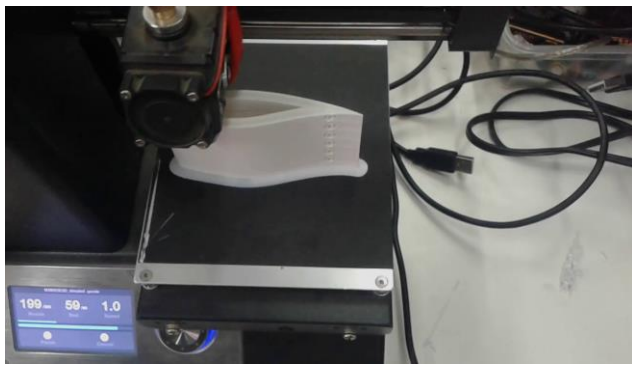


Figure 32: Printing 3D Model of the blade airfoil with Dimples config. #II



Figure 33: Dimpled S830 Model with Dimples config. #II in Test Section

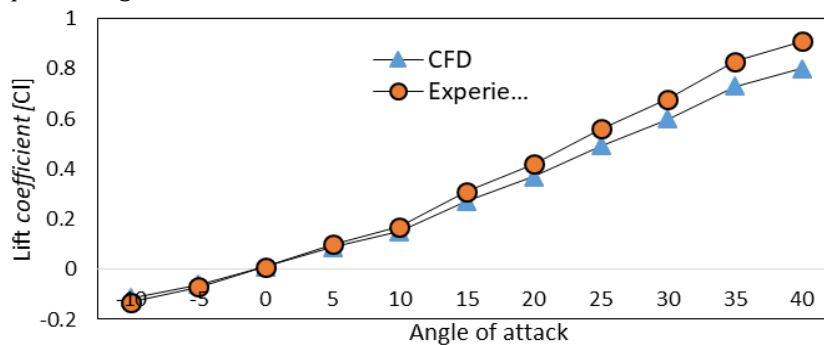


Figure 34: Comparison of Experimental and Numerical Analysis result of Lift coefficient for S830 Airfoil blade model

7. CONCLUSION

Based up on the specific site wind phenomena and BEM method HAWT blade is designed for cut in, rated & cut off wind speed of 3m/s,10m/s and 22 m/s respectively. The tip speed ratio of 6.8 and radius of 25 m was selected. NREL’s airfoil S830 is selected for blade profile from aerodynamics performance comparison among different airfoils. The chord distribution from root to tip ranges between 3.39m to 0.77m, while angle of twist ranges from 31.14° – 3.73°.

The aerodynamic performance of the designed blade was evaluated using LES. Maximum aerodynamics performance of the blade occurs at an angle of attack of 12°. At angle of attack higher than 15° flow separation occur at pressure side of the baseline blade. This adverse phenomena will lessen the efficency of the Turbine. Based up on the cetin correlation the power extraction coefficient of designed base model blade is found to be 0.41.

Among the examined dimples configurations aerodynamic performance of config #2 (i.e. 58 Inward dimple on the suction surface with a diameter of 10 cm at 0.4 chord length with 10 cm spacing between them) show a very good enhancement than others with a maximum reachable Angle of attack of 17°. At a rated wind speed of 10 m/s; By using Cetin’s correlation the power extraction coefficient of Config#2 were found to be 0.4415. The first model (Config#1) 55 outward dimples with a diameter of 10 cm at a chord length ratio of 0.5 were imparted. The result of model one explicate clearly that outward dimple will not delay flow separation for wind turbine blades rather they will induce additional drag force on the blade; with maximum aerodynamic performance of 6.9 which is lesser than the baseline. The aerodynamic performance of Model six (10cm inward dimples at the suction surface and 5 cm inward dimple at the pressure side) enhanced the aerodynamic performance of the baseline blade to 9.93, while the remaining three configuration have small enhancement which is approach to 1%. To validate the result of computational work on effect of dimples, experiments were carried out at small scaled S830 airfoil using subsonic wind tunnel. By varying the Reynold number six different experiments were done for both dimpled and Baseline models. The experiment result show that dimples will increase the aerodynamic performance by delaying flow separation.

REFERENCE

1. Usha Rao K. & Kishore VVN. (2009). Wind Power Technology Diffusion Analysis in Selected States of India. *Renewable Energy*; 34: 983–88
2. Betz A. (1935) .*Applied Airfoil Theory: a general review of progress* Volume IV, Division 1st edition, McGraw-Hill.
3. Frank M. White (2009). Fluid Mechanics, Sixth Edition, *McGraw-Hill*
4. Deepenshu Srivastav (2012). Flow control over airfoils using different shaped dimples. *International Conference on Fluid Dynamics and Thermodynamics Technologies (FDTT) IPCSIT, Volume 33, IACSIT Press, Singapore.*
5. Livya. E, Anitha. G, Valli. P, (2015). Aerodynamic analysis of dimple effect over aircraft wing, *International journal of mechanical aerospace industrial and mechatronics engineering, Volume 9. Number 2, Pages 350-353.*
6. Mulugeta Biadgo, (2009), "Computer-aided aerodynamic and structural design of horizontal- axis wind turbine blades", M.Sc. Thesis Addis Ababa University, Addis Ababa.
7. Haseeb S., Boorsma K., Kim C, and cho T., (2011). Analysis of detailed aerodynamics measure on a 4.5 m diameter rotor placed in the large German Dutch wind tunnel DNW. *In proceedings of EWEA, Brussels, Belgium.*
8. Peter J. Schubel and Richard J. Crossley, (2012) "Wind Turbine Blade Design", University of Nottingham, Nottingham NG7 2RD, UK.
9. Serhat Duran, (2005) "Computer- Aided design of Horizontal- axis wind turbine blades", Middle east technical university.
10. Port-Agel, F., Wu, Y.-T., Lu, H., & Conzemius, R. J. (2011). Large-eddy Simulation of Atmospheric Boundary Layer Flow through Wind Turbines and Wind Farms. *Journal of Wind Engineering and Industrial Aerodynamics*, 99, 154-168.
11. Arun K.K., Deepanshu K., Srivastav J. (2018). Analyzing the effect of dimples on wind turbine efficiency using CFD. *International Journal of Applied Engineering Research*, 13(6): pp. 4484-4489.
12. Burger C. & Hartfield R. (2006). Wind turbine airfoil performance optimization using the vortex lattice method and genetic algorithm. *4th AIAA Energy Conversion Engineering Conference AIAA 2006-4051*, 26-29.
13. Hansen and Butterfield C. (1993). Aerodynamics of horizontal-axis wind turbines. *1st edition, McGraw-Hill.*